Electronic Supplementary Information

Efficient and selective removal of Pb^{2+} from aqueous solution by using a O^- functionalized metal-organic framework

Wen Jiang,[a,‡] Cai-Xia Yu,[a,‡,*] Ming-Xuan Yu,[a] Jing Ding,[a] Jian-Guo Song,[a] Xue-Qin Sun[a] and Lei-Lei Liu[a,*]

[a] School of Environmental and Material Engineering, Yantai University, Yantai 264005, P. R. China

‡ The first two authors contributed equally.

* To whom correspondence should be addressed. E-mail addresses: liuleileimail@163.com (L.-L. Liu).

Experimental Section

General Procedure. Ligand H_2ADB was prepared according to the literature method.[1] All other chemicals and reagents were obtained from commercial sources and used as received. Powder X-ray diffraction (PXRD) was performed using a PANalytical X'Pert PRO MPD system (PW3040/60). Thermal analysis was performed with a Netzsch STA-449F3 thermogravimetric analyzer at a heating rate of 10 °C min^{-1} and a flow rate of 20 cm^3 min^{-1} (N_2). Fourier transform infrared (FT-IR) spectra were recorded on an IR Prestige-21. The FT-IR samples were prepared by blending compound with KBr and compressing the mixture to obtain transparent sheets. X-ray photoelectron spectroscopy (XPS) was performed on a Thermo Escalab 250 spectrometer with monochromated $Al_{K\alpha}$ excitation. The zeta potential was determined using dynamic light scattering (DLS) on Malvern Instruments Nanosizer-ZS90.

X-ray crystal structure determination. Single X-ray diffraction intensities of crystal were collected on a CCD diffractometer at 296 K. All diffractometers were equipped with a graphite monochromated Mo-Kα radiation (λ = 0.71073). The structure was solved by direct method and expanded with Fourier technique. All calculations were performed with SHELXL-97 package. All H atoms in **Pr-MOF** were placed in geometrically idealized positions and constrained to ride on their parent atoms. The crystal data for **Pr-MOF** was summarized as follows: $C_{25}H_{21}N_4O_{8.5}Pr$, Mr = 654.36, monoclinic, space group $P2_1/n$, a = 16.455(3) Å, b = 8.7878(18) Å, c = 20.761(4) Å, α = 90°, β = 93.15(3)°, γ = 90°, V = 2997.6(10) $Å^3$, Z = 4, D_c = 1.468 g cm^{-3}, $F(000)$ = 1320.0 and μ = 1.678 mm^{-1}, 29334 reflections collected, 5276 unique (R_{int} = 0.0532). R_1 = 0.0358, wR_2 = 0.0887 and S = 1.064.

Adsorption experiments. The adsorption kinetics data were fitted with different kinetic models, pseudo first-order model, pseudo-second-order, expressed as follows:

$$\ln(q_e - q_t) = \ln q_e - k_1 t \quad (1)$$

$$\frac{t}{q_t} = \frac{1}{k_2 q_e^2} + \frac{t}{q_e} \quad (2)$$

where q_t (mg g^{-1}) and q_e (mg g^{-1}) are the adsorption capacity at any time t (min) and at equilibrium; k_1 (min^{-1}) and k_2 (g mg^{-1} min^{-1}) are kinetic rate constants for the pseudo-first-order and pseudo-second-order models, respectively.

The Langmuir and Freundlich isotherm model were employed to simulate the adsorption isotherm data and can be described as:

$$\frac{C_e}{q_e} = \frac{C_e}{q_m} + \frac{1}{q_m K_L} \quad (3)$$

$$\ln q_e = \ln K_F + \frac{1}{n} \ln C_e \quad (4)$$

where q_e (mg g^{-1}) is the adsorption amounts at equilibrium and C_e (mg L^{-1}) is the equilibrium concentration of Pb(II). q_m (mg g^{-1}) is the maximum amount or the saturated adsorption amount. K_L (L mg^{-1}) is the Langmuir constant, quantitatively reflecting the affinity of binding sites to energy of adsorption. K_F ((mg g^{-1})/(L $mg^{-1})^{1/n}$) is the Freundlich constant which indicates the adsorption capacity and n is an empirical parameter related to the intensity of adsorption. The Langmuir model assumes that the solid surface active sites can be occupied only by one layer of adsorbates and there is no interaction between the adsorbate molecules. On the contrary, the Freundlich model is based on a heterogeneous adsorption.

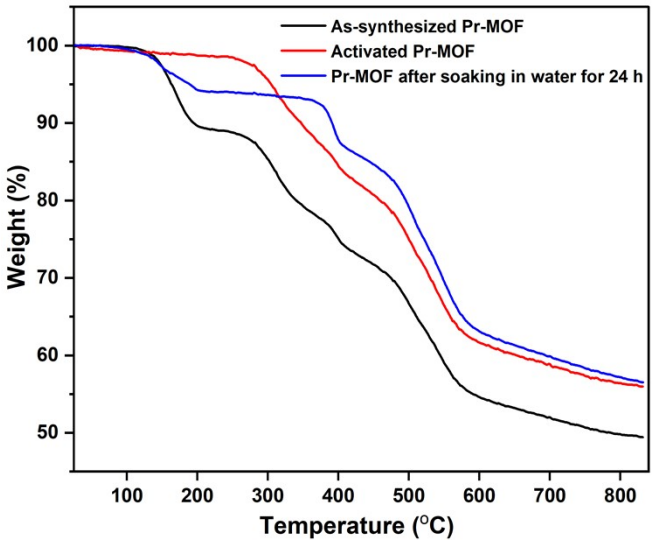

Figure S1. TGA curves of the as-synthesized **Pr-MOF**, activated **Pr-MOF** and **Pr-MOF** after soaking in water for 24 h.

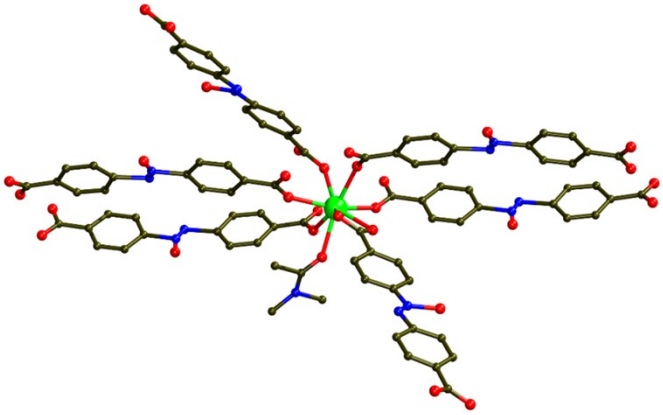

Figure S2. Coordination environment of Pr(III) atom in **Pr-MOF**.

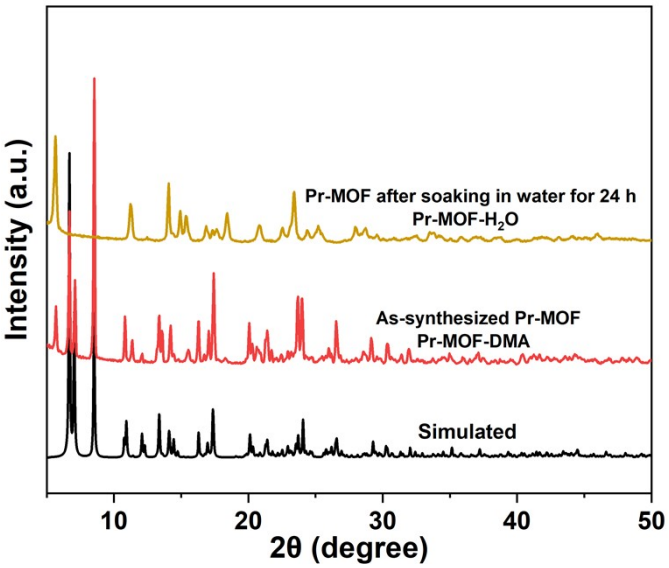

Figure S3. PXRD patterns of the simulated, as-synthesized **Pr-MOF** and **Pr-MOF** after soaking in water for 24 h.

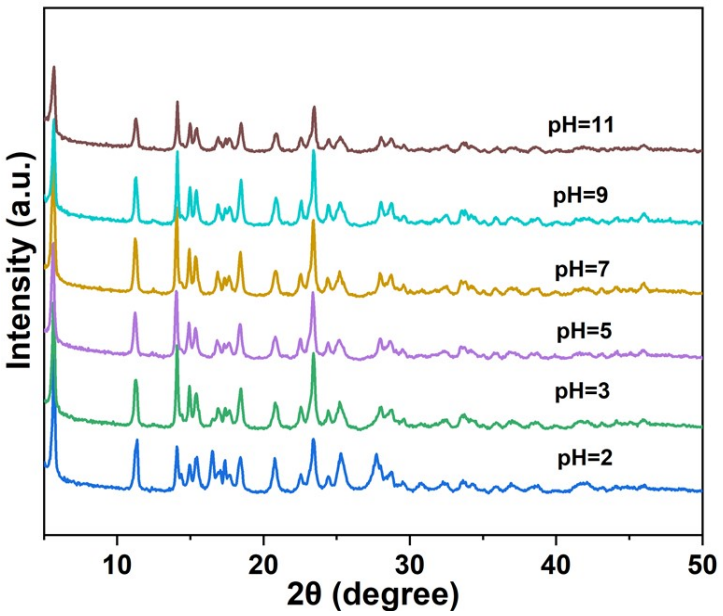

Figure S4. PXRD patterns of **Pr-MOF** after soaking in water (24 h) for different pH values.

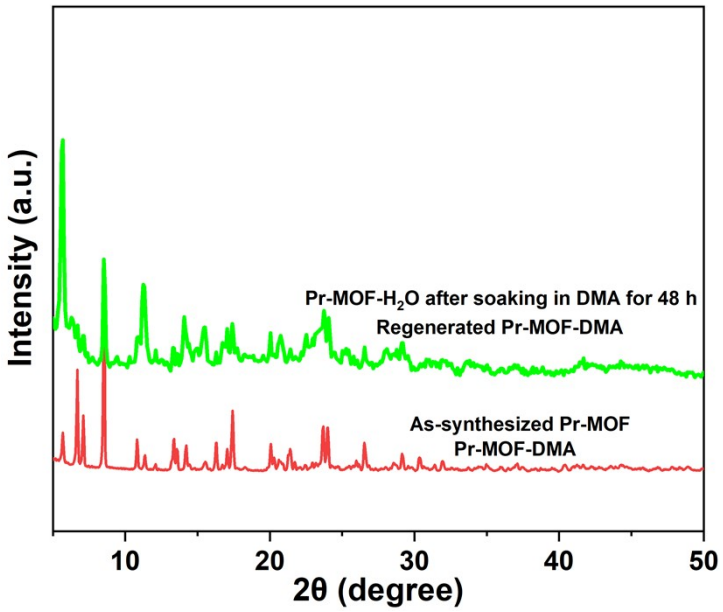

Figure S5. PXRD patterns of as-synthesized **Pr-MOF** and **Pr-MOF-H_2O** after soaking in DMA for 48 h.

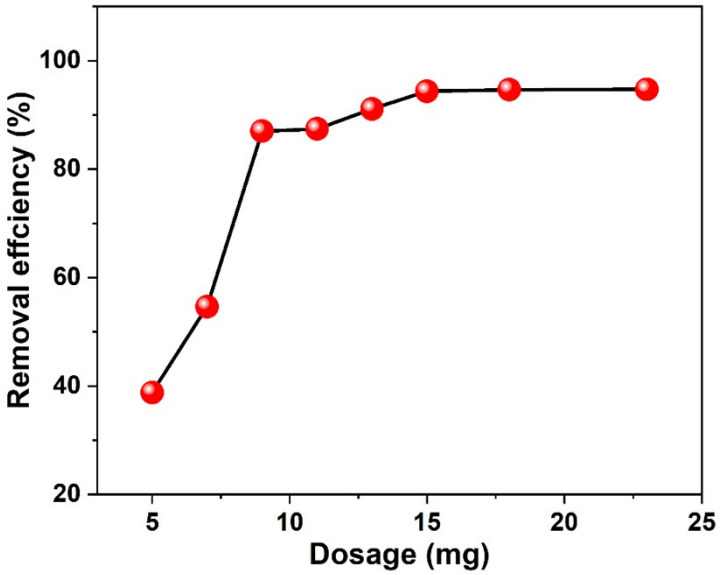

Figure S6. Effect of **Pr-MOF** dosage on the removal of Pb^{2+}. C_0 = 60 ppm, V = 50 mL, pH = 6 and T = 298 K.

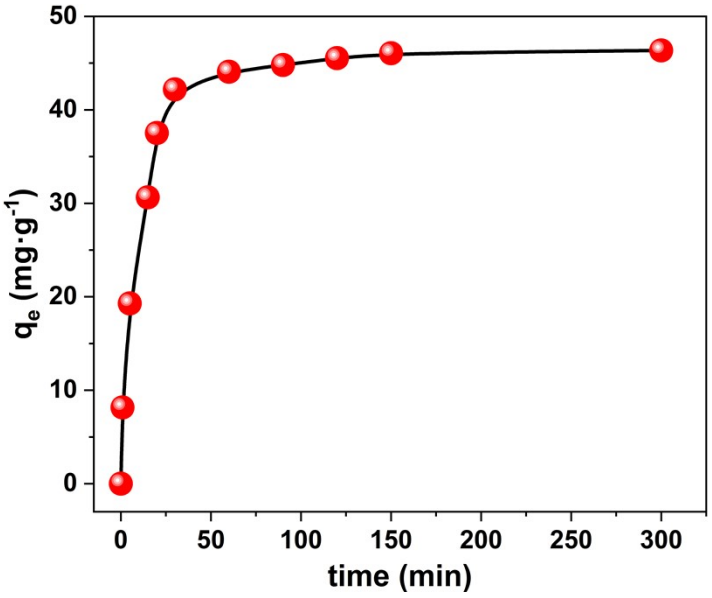

Figure S7. Influences of adsorption time on adsorption. C_0 = 10 ppm, $m_{adsorbent}$ = 9 mg, V = 50 mL, pH = 6.0, and T = 298 K.

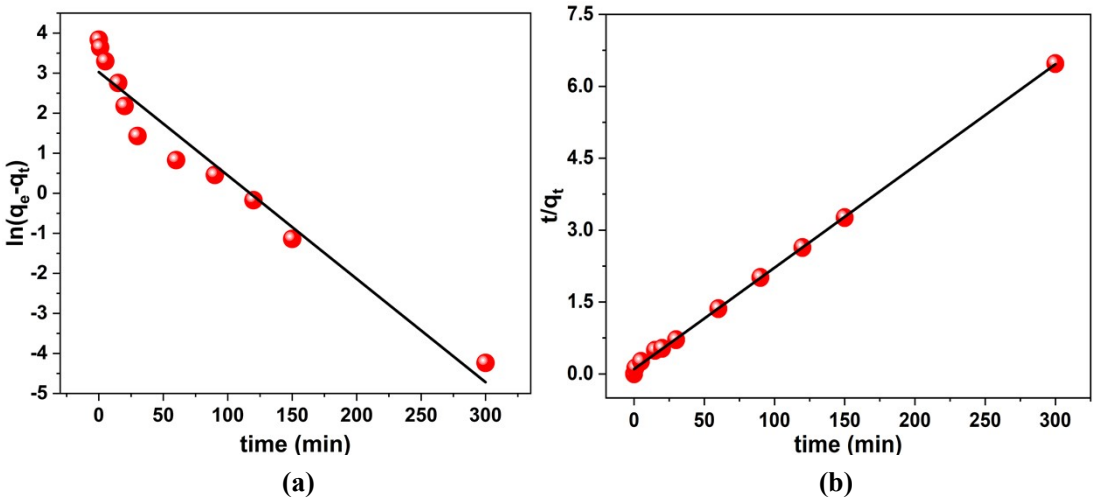

Figure S8. (a) Pseudo-first-order kinetic model and (b) Pseudo-second-order kinetic model.

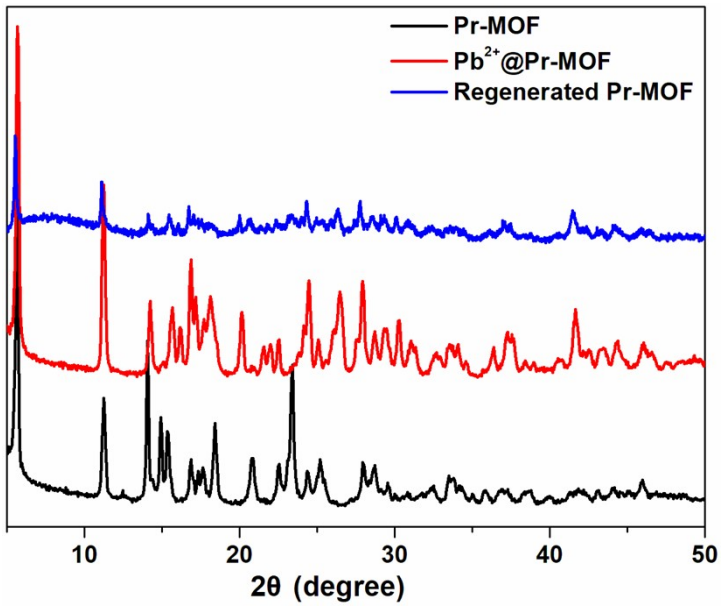

Figure S9. The PXRD patterns of **Pr-MOF**, Pb^{2+}@**Pr-MOF** and the recovered samples after four cycles of adsorption-desorption experiments.

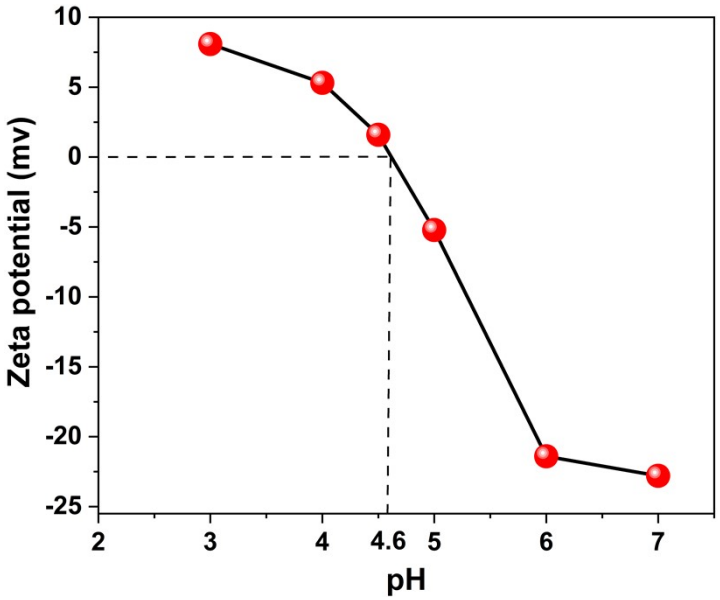

Figure S10. The effect of pH on zeta potentials of **Pr-MOF**.

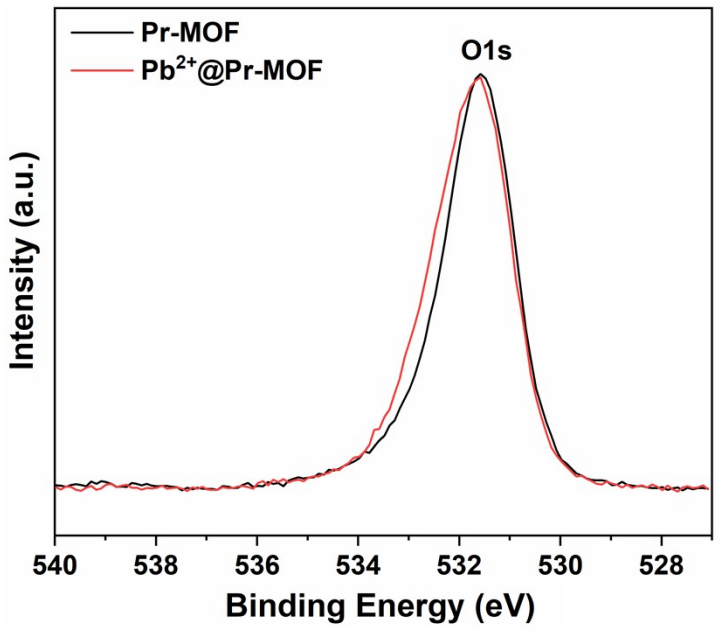

Figure S11. O 1s spectra before and after Pb^{2+} adsorption.

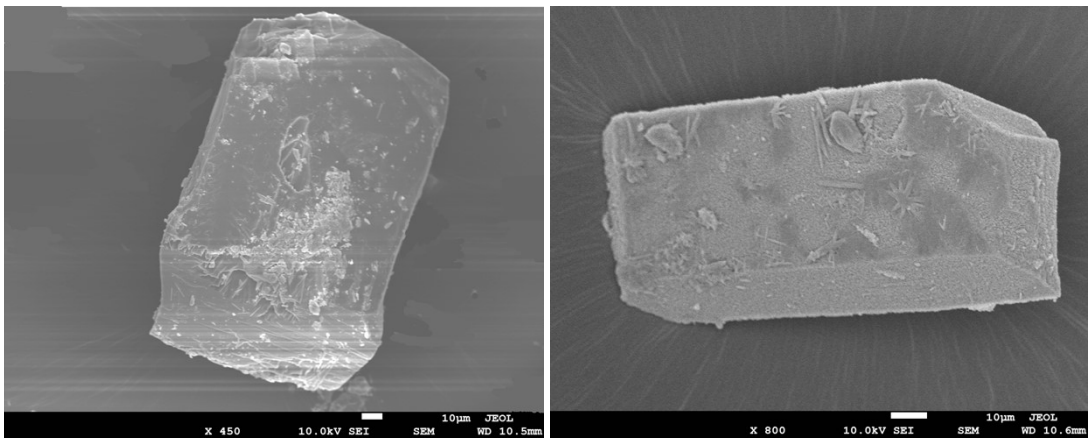

(a) **(b)**

Figure S12. The SEM images of (a) **Pr-MOF** and (b) **Pr-MOF** after soaking in H_2O for 24 h.

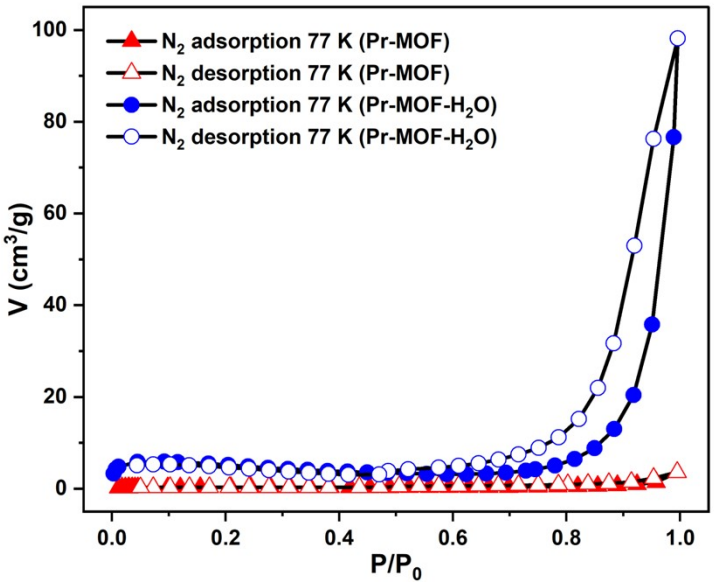

Figure S13. Gas adsorption isotherms of as-synthesized **Pr-MOF** and **Pr-MOF** after soaking in water for 24 h.

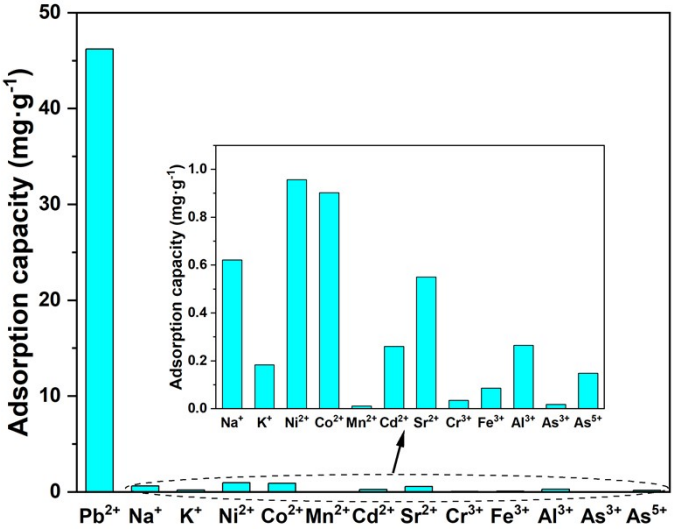

Figure S14. Selective adsorption of **Pr-MOF** for different metal ions. T = 298 K, C_0 = 10 ppm, pH = 6, $m_{adsorbent}$ = 9 mg and V = 50 mL. Based on the K_{sp} values of $[Al(OH)_3]$ (1.3×10^{-33}), $[Cr(OH)_3]$ (6.3×10^{-31}) and $[Fe(OH)_3]$ (4.0×10^{-38}), the metal ions of Al^{3+}, Cr^{3+} and Fe^{3+} are easily subject to precipitation at the tested pH of 6.0, and the residual concentration of these metal ions were calculated to be 3.51×10^{-5} ppm for Al^{3+}, 3.28×10^{-2} ppm for Cr^{3+} and 2.23×10^{-9} ppm for Fe^{3+}, respectively. Thus, the selective measurements for Al^{3+}, Cr^{3+} and Fe^{3+} were tested in a single system, with a solution pH of 4.0 for Al^{3+}, 5.0 for Cr^{3+} and 2.0 for Fe^{3+}, to guarantee concentration of these metal ions in solution is 10 ppm.

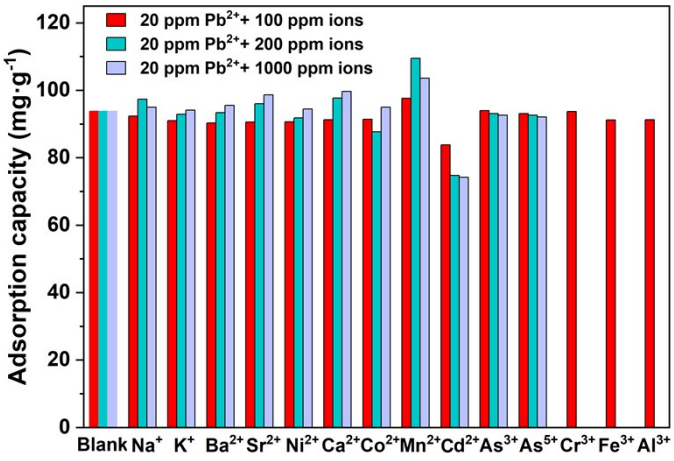

Figure S15. The effects of competing ions on Pb^{2+} removal by **Pr-MOF**. The anti-interference experiment was performed at pH of 6.0 to evaluate the effect of the presence of the interference ions on Pb^{2+} adsorption. For the metal ions of Al^{3+}, Cr^{3+} and Fe^{3+}, they are easily subject to precipitation at the tested pH of 6.0. Based on the K_{sp} value for each ion ($K_{sp}[Al(OH)_3] = 1.3 \times 10^{-33}$, $K_{sp}[Cr(OH)_3] = 6.3 \times 10^{-31}$ and $K_{sp}[Fe(OH)_3] = 4.0 \times 10^{-38}$), the residual concentrations of Al^{3+}, Cr^{3+} and Fe^{3+} at pH 6.0 were calculated to be 3.51×10^{-5} ppm, 3.28×10^{-2} ppm and 2.23×10^{-9} ppm, respectively. Thus, the anti-interference experiment for these metal ions was investigated at pH 6.0, with a concentration of 3.51×10^{-5} ppm for Al^{3+}, 3.28×10^{-2} ppm for Cr^{3+} and 2.23×10^{-9} ppm for Fe^{3+}. As shown in Fig. S15, negligible effect was posed on Pb^{2+} adsorption by Al^{3+}, Cr^{3+} and Fe^{3+}.

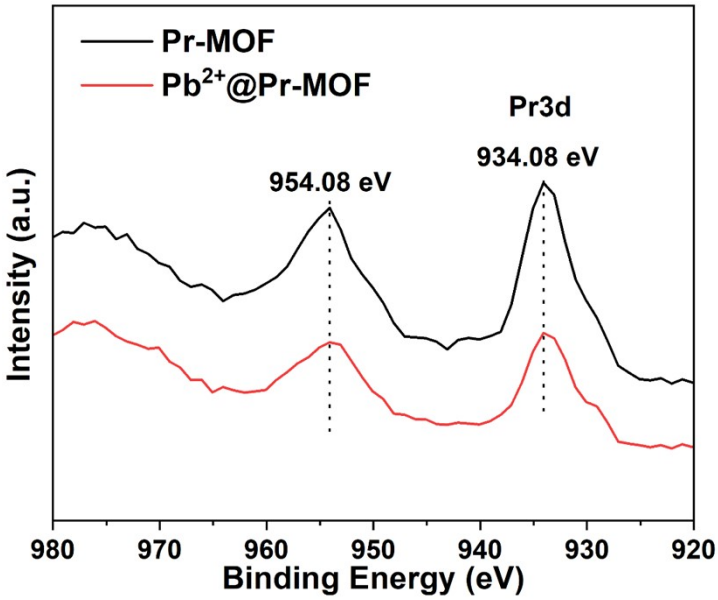

Figure S16. Pr 3d XPS spectrum of **Pr-MOF** and Pb^{2+}@**Pr-MOF**.

Table S1. Adsorption constants for Langmuir and Freundlich isotherm models.

Langmuir			Freundlich		
q_{max}	K_L	R^2	K_F	n	R^2
584.79	0.0848	0.999	74.652	0.403	0.825

Table S2. Comparison of Pb^{2+} maximum uptake capacity for **Pr-MOF** with other adsorbents.

Adsorbents	Maximum uptake capacity (mg g^{-1})	References
Cu-BTC-Th	732.86	2
Fe doped HKUST-1	565	3
Pr-MOF	**560.26**	**this work**
Tb-MOF	547	4
Zn-MOF	463.52	5
Co-Al-LDH@Fe_2O_3/DPCNF	426.76	6
AMCA-MIL-53(Al)	390	7
Cu-BTC	333	8
Zn-BTC	312	8
Fe_3O_4/MIL-96(Al)	301.5	9
Fe_3O_4@ZIF-8	276.06	10
MIL-101(Fe)/GO	128.6	11
DUT-67	98.5	12
CMP-3a	93.2	13
Cd-MOF	60.857	14

Table S3. Kinetic parameters for adsorption of Pb^{2+}.

		Pseudo-first-order model			Pseudo-second-order model		
T/K	$q_{e,exp}$	k_1	$q_{e,cal}$	R^2	k_2	$q_{e,cal}$	R^2
298	46.356	0.0258	20.655	0.951	0.0046	47.148	0.999

References

(1) Reid, E. B.; Pritchett, E. G. p, p′-azoxy and p, p′-azo-dibenzoic acids. *J. Org. Chem.* **1953**, *18*, 715–719.

(2) Zhong, J.; Zhou, J.; Xiao, M.; Liu, J.; Shen, J.; Liu, J.; Ren, S. Design and Syntheses of Functionalized Copper-Based MOFs and Its Adsorption Behavior for Pb(II). *Chinese Chem. Lett.* **2022**, *33*, 973–978.

(3) Goyal, P.; Paruthi, A.; Menon, D.; Behara, R.; Jaiswal, A.; V, K.; Kumar, A.; Krishnan, V.; Misra, S. K. Fe Doped Bimetallic HKUST-1 MOF with Enhanced Water Stability for Trapping Pb(II) with High Adsorption Capacity. *Chem. Eng. J.* **2022**, *430*, 133088.

(4) Zhu, H.; Yuan, J.; Tan, X.; Zhang, W.; Fang, M.; Wang, X. Efficient Removal of Pb^{2+} by Tb-MOFs: Identifying the Adsorption Mechanism through Experimental and Theoretical Investigations. *Environ. Sci. Nano* **2019**, *6*, 261–272.

(5) Yu, C. X.; Wang, K. Z.; Li, X. J.; Liu, D.; Ma, L. F.; Liu, L. L. Highly Efficient and Facile Removal of Pb^{2+} from Water by Using a Negatively Charged Azoxy-Functionalized Metal-Organic Framework. *Cryst. Growth Des.* **2020**, *20*, 5251–5260.

(6) Poudel, M. B.; Awasthi, G. P.; Kim, H. J. Novel Insight into the Adsorption of Cr(VI) and Pb(II) Ions by MOF Derived Co-Al Layered Double Hydroxide @hematite Nanorods on 3D Porous Carbon Nanofiber Network. *Chem. Eng. J.* **2021**, *417*, 129312.

(7) Alqadami, A. A.; Khan, M. A.; Siddiqui, M. R.; Alothman, Z. A. Development of Citric Anhydride Anchored Mesoporous MOF through Post Synthesis Modification to Sequester Potentially Toxic Lead(II) from Water. *Microporous Mesoporous Mater.* **2018**, *261*, 198–206.

(8) Hasankola, Z. S.; Rahimi, R.; Safarifard, V. Rapid and Efficient Ultrasonic-Assisted Removal of Lead(II) in Water Using Two Copper- and Zinc-Based Metal-Organic Frameworks. *Inorg. Chem. Commun.* **2019**, *107*, 107474.

(9) Mehdinia, A.; Jahedi Vaighan, D.; Jabbari, A. Cation Exchange Superparamagnetic Al-Based Metal Organic Framework (Fe_3O_4/MIL-96(Al)) for High Efficient Removal of Pb(II) from Aqueous Solutions. *ACS Sustain. Chem. Eng.* **2018**, *6* (3), 3176–3186.

(10) Wang, M.; Zhao, Z.; Lin, S.; Su, M.; Liang, B.; Liang, S. New Insight into the Co-Adsorption of Oxytetracycline and Pb(II) Using Magnetic Metal-Organic Frameworks Composites in Aqueous Environment: Co-Adsorption Mechanisms and Application Potentials. *Environ. Sci. Pollut. Res.* **2022**, doi: 10.1007/s11356-022-19339-z.

(11) Lu, M.; Li, L.; Shen, S.; Chen, D.; Han, W. Highly Efficient Removal of Pb^{2+} by a Sandwich Structure of Metal-Organic Framework/GO Composite with Enhanced Stability. *New J. Chem.* **2019**, *43*, 1032–1037.

(12) Geisse, A. R.; Ngule, C. M.; Genna, D. T. Removal of Lead Ions from Water Using Thiophene-Functionalized Metal-Organic Frameworks. *Chem. Commun.* **2019**, *56*, 237–240.

(13) Qiao, X. X.; Liu, G. F.; Wang, J. T.; Zhang, Y. Q.; Lü, J. Highly Efficient and Selective Removal of Lead Ions from Aqueous Solutions by Conjugated Microporous Polymers with Functionalized Heterogeneous Pores. *Cryst. Growth Des.* **2020**, *20*, 337–344.

(14) Yu, C.; Han, X.; Shao, Z.; Liu, L.; Hou, H. High Efficiency and Fast Removal of Trace Pb(II) from Aqueous Solution by Carbomethoxy-Functionalized Metal-Organic Framework. *Cryst. Growth Des.* **2018**, *18*, 1474–1482.